Statistical neutron capture in the limit of low nuclear level density

J. R. Winkelbauer, S. M. Mosby, A. Couture, H. Y. Lee, J. L. Ullmann, T. Kawano, G. Rusev, and M. Jandel*
Los Alamos National Laboratory, Los Alamos, New Mexico 87545, USA

M. Krtička
Charles University in Prague, CZ-180 00 Prague 8, Czech Republic

(Received 11 September 2018; published 25 February 2019)

A major barrier in the study of neutron-induced nuclear reactions is the impossibility of direct measurements with short-lived radioactive isotopes. For these exotic nuclei, theoretical inputs such as the photon strength function (PSF) are poorly constrained. At Los Alamos National Laboratory, the Detector for Advanced Neutron Capture Experiments (DANCE) provides direct measurements of γ-ray cascades following neutron capture reactions on stable or long-lived radioactive nuclei. While Hauser-Feshbach calculations can provide reasonable predictions for neutron capture on heavy nuclei, their application to neutron-rich light nuclei with low nuclear level densities and low neutron separation energies is questionable. In this paper, we report on the γ-ray spectra from individual neutron resonances from the ^{96}Zr(n,γ) reaction, with an emphasis on the sensitivity of of the γ-ray spectra to different PSF models. The comparison of the measured γ-ray spectra with predicted spectra does not support the addition of a low-energy enhancement of the size reported in many charged-particle reaction measurements, but the sensitivity of the γ-ray spectra to different PSF models is weak.

DOI: 10.1103/PhysRevC.99.024318

I. INTRODUCTION

Radiative capture of neutrons on neutron-rich nuclei continues to be an active area of research. Understanding the astrophysical *r*-process requires accurate predictions of neutron-capture rates for target nuclei far from stability where direct measurements are impossible. *R*-process reaction network calculations rely on theoretical predictions of neutron capture rates, and different statistical-model-code predictions may differ by several orders of magnitude when calculating rates far from stability [1–3]. Clearly, improvement in the theoretical treatment of neutron capture is needed, particularly for unstable isotopes where model parameters are unconstrained.

The neutron-capture process is typically modeled as a compound reaction for energies up to a few MeV; the neutron and the target nucleus combine in a well-defined, unbound state of the residual nucleus, which can then decay by γ-ray emission, neutron emission, or fission. The probability for the radiative neutron capture process is given by the product of the probability of the formation of the compound nucleus and the probability of γ-ray emission; the formation and decay are treated independently. This concept allows for the investigation of the γ-ray emission probability using reactions other than neutron capture. The photon strength function (PSF) contains the energy dependence of the γ-ray emission probability which is dominated by the low-energy tail of the $E1$ giant dipole resonance (GDR). The most traditional representation of the E1 PSF starts with a simple Lorentzian function [4], which has since been modified at low energies as the generalized Lorentzian (GLO) form, which allows for a energy-dependent width and an additional term that explicitly defines the PSF for $E_\gamma = 0$ [5].

The precise behavior of the PSF for energies well below the neutron separation energy has seen renewed interest due to an influx of charged-particle induced measurements which find a large enhancement over typical model predictions. The numerous measurements where the strength function was extracted in charged particle induced reactions (see Refs. [6–8] as a few examples) have found a low-energy enhancement, while measurements where the strength function was studied using neutron induced reactions [9–11] are not consistent with a very large low-energy enhancement. Significant effort has been invested to understand the limitations of these charged particle induced reaction studies, such as in the Oslo method [12], while these experiments become more and more common at experimental facilities. The Oslo-type low-energy enhancement of the PSF would have significant effects on neutron capture predictions far from stability, as the neutron separation energy becomes lower [13]. In order for indirect methods such as the Oslo method to be useful for these nuclei, it is necessary to understand how well the statistical model describes neutron capture reactions for these nuclei with low level density.

The goal of this study is to understand if useful information about the strength function can be extracted from a nucleus which has a relatively small number of levels below the neutron separation energy. Many future indirect studies of neutron capture will apply the extreme statistical model to nuclei with very low neutron separation energies and to nuclei near shell closures. This publication presents the results

*Present address: Department of Physics and Applied Physics, University of Massachusetts Lowell, Lowell, MA 01854, USA.

 ©2019 American Physical Society

TABLE I. Isotopic composition of the Zr sample.

	^{96}Zr	^{94}Zr	^{92}Zr	^{91}Zr	^{90}Zr
Composition (%)	86.4	4.0	2.7	1.9	5.0
(n,γ) Q value (MeV)	5.575	6.462	6.734	8.634	7.194

from the ^{96}Zr(n,γ) reaction, where the nuclear level density is very low, and discusses the shortcomings of using the statistical model to describe this reaction.

II. EXPERIMENTAL DETAILS

The ^{96}Zr(n,γ) reaction was studied using the Detector for Advanced Neutron Capture Experiments (DANCE) [14], which is located on flight path 14 at the Lujan Neutron Scattering Center [15], which uses the Los Alamos Neutron Science Center (LANSCE) linear proton accelerator to produce neutrons from a tungsten spallation target. Flight path 14 originates from the upper-tier water moderator of the tungsten target, and while the Lujan Center primarily focuses on material science, this flight path is optimized for studying neutron capture reactions from thermal up to 10–100 keV neutron energy. Proton pulses from the LANSCE accelerator drive the Lujan target at a rate of 20 Hz, so time-of-flight can be used to measure incident neutron energy.

DANCE consists of 160 close-packed BaF_2 crystals which are backed with photomultiplier tubes. The array was designed to maximize geometric efficiency, so the only dead areas in the array are to allow the beamline to pass through. The DANCE crystals were designed to comprise a shell of BaF_2 with an inner radius of 17 cm and a thickness of 15 cm. DANCE has a total γ-ray detection efficiency of over 80% up to 8 MeV for a single γ-ray, and a peak/total efficiency of over 50% up to 8 MeV [14,16]. A spherical shell of ^{6}LiH is located inside of DANCE to absorb neutrons scattered from the sample. DANCE is instrumented with a fully digital data acquisition system, which allows for pulse-shape discrimination, which is necessary to filter out events arising from radium contamination in the BaF_2. The spread in time for multiple γ-rays detected in a single capture event can be a few nanoseconds, so a 10-ns coincidence window is used to cluster multiple detector signals together in the offline data analysis. The high granularity and close packed geometry of DANCE allows γ-rays which deposit energy into more than one adjacent crystal to be combined into "cluster" energies, which are more representative of the emitted γ-ray energy. The γ-ray cascade spectra are then categorized by the multiplicity of clusters, M_{cl}. For the *multistep cascade spectrum* with cluster multiplicity $M_{\rm cl}$, each of the $M_{\rm cl}$ cluster energies are added individually to the histogram.

A powder of ZrO_2 was pressed into a 5-mm-diameter pellet which was then captured between two sheets of kapton tape. The total mass of Zr illuminated by the neutron beam was $\approx$120 mg, and the isotopic composition is listed in Table I. Because DANCE has a high efficiency to detect high multiplicity γ-ray cascades, the analysis can be restricted to cascades where the full capture Q value was registered. By requiring the appropriate Q value and limiting the analysis to known resonances in ^{96}Zr, much of the isotopic contamination was removed.

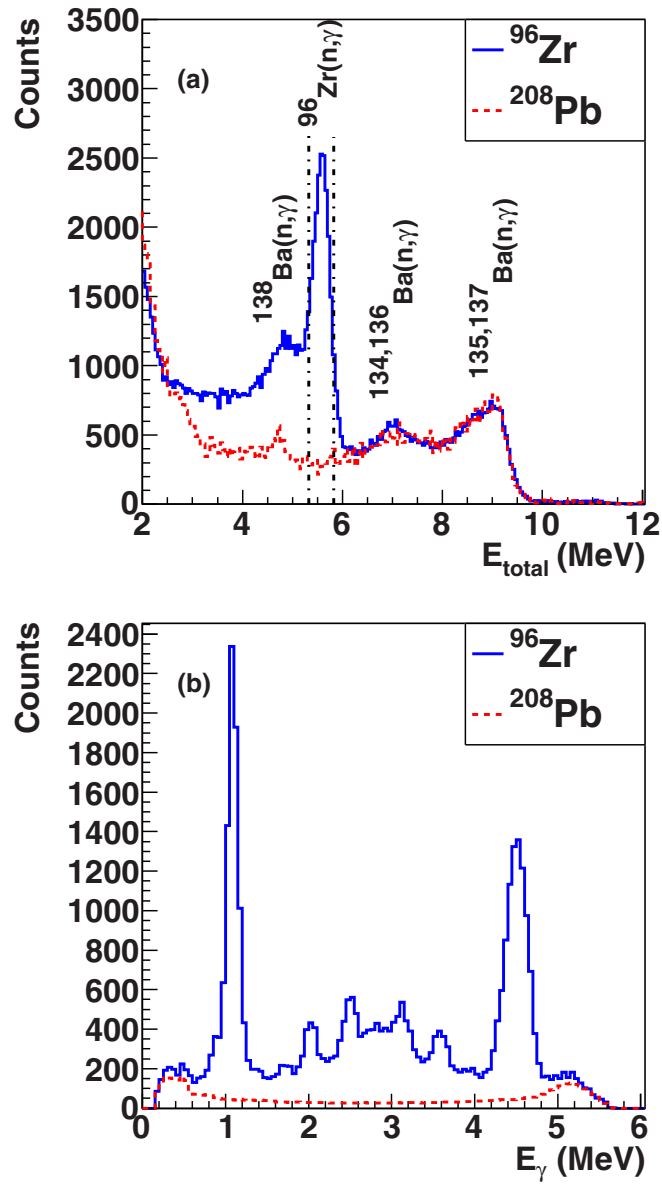

FIG. 1. (a) Total γ-ray energy spectrum for the ^{96}Zr sample (in blue) and for the ^{208}Pb sample (in red), for events with $M_{\rm cl} = 2$. (b) Multistep-cascade spectrum for events with $M_{\rm cl} = 2$ that fall into the $E_{\rm total}$ cut shown in the upper figure. Both panels show data for the ^{96}Zr(n,γ) resonance at 3818 eV.

III. DATA REDUCTION

The data reduction involves removing backgrounds and contaminations. The most significant source of background comes from scattered neutrons which are captured on Barium isotopes in the DANCE crystals which result in a γ-ray cascade with a total measured γ-ray energy, $E_{\rm total}$, near the ^{96}Zr neutron capture Q value. For certain resonances, there is small contamination from neutron capture on other Zr isotopes in

the sample. The lighter Zr isotopes have capture Q values that are larger than that of ^{96}Zr (see Table I), so cascades that are partially deposited in DANCE can contaminate the Q-value cut for ^{96}Zr.

To quantify the background that comes from neutrons scattered from the sample, a ^{208}Pb sample was measured during the same LANSCE run cycle using the DANCE array, and the procedure described in Ref. [17] was used. The contribution of the background needs to be normalized for each neutron-energy resonance. To extract the normalization factor, the ^{208}Pb background is scaled to match the integral number of events with 8 MeV $< E_{\text{total}} <$ 10 MeV as in the ^{96}Zr data, for each resonance. Figure 1 illustrates this procedure for one strong resonance at 3.818 keV; the upper panel shows the E_{total} spectrum which is used to normalize the background data to the foreground data, and the lower panel shows the corresponding multistep-cascade spectrum with a $\pm$0.25 MeV wide cut around the Q-value. In the upper panel, peaks at 4.7, 8.6, 6.9, 9.1, and 7.0 MeV correspond to scattered neutrons which capture on ^{138}Ba, ^{137}Ba, ^{136}Ba, ^{135}Ba, and ^{134}Ba, respectively, in the BaF_2 DANCE crystals. The capture of scattered neutrons causes a background without distinct features in the cascade spectrum, compared to the foreground data where you can see transitions to individual known levels in ^{97}Zr, as shown in the lower panel of Fig. 1. This procedure is used to quantify and subtract the scattered neutron background for each resonance that was studied. For the ^{96}Zr ($Q = 5.575$ MeV) resonance at 4.133 keV, the 4.118 keV resonance from ^{92}Zr ($Q = 6.734$ MeV) partially overlaps in neutron time-of-flight, so a subtraction was made using data from a ^{92}Zr enriched sample, using the same procedure as with the ^{208}Pb sample. The measured multistep-cascade spectra can then be compared to predicted γ-ray cascades using different PSF models, after processing the calculated cascades through a well-exercised GEANT4 simulation [14].

IV. EXPERIMENTAL RESULTS

The cascade spectra from seven well-resolved resonances in ^{96}Zr are shown in Fig. 2. The positions and spin/parities of the capture states are taken from Ref. [18], shown in Table II, and resonances up to 18 keV were measured. The resonance at 870 eV reported in Ref. [18] was not observed, which was also absent in Ref. [19]. The resonances which do not have assignments in Ref. [18] are not shown in the present work, because independently determining the J^π of these resonances is difficult. In addition, the resonances at 15.138 keV and 15.419 keV are not included because they were not resolved in incident neutron time-of-flight. The γ-ray cascades are dominated by one, two, and three-step cascades, due to the low level density in ^{97}Zr. Figure 2 shows the cascades for two and three step cascades which result from a detected E_{total} that falls within $\pm$250 keV of the capture Q value, as indicated in Fig. 1. In this measurement there is only one cleanly measured s-wave resonance at 5443 eV, which is shown in the bottom panels of Fig. 2. It is not surprising that the s-wave capture does not strongly populate the two low lying states, as the p-wave capture does in the middle and top panels. The known states in ^{97}Zr below 2 MeV have positive parity, so $M1/E2$ transitions to the lower excited states are suppressed in favor of an $E1$ transition to a state above 2 MeV, because the $E1$ PSF should dominate for these energies. It appears that each resonance only populates a few discrete states, as opposed to a continuum of states. For the capture states with $J^\pi = 1/2^-$, the most likely two-step cascade is through the first excited state at 1103 keV ($3/2^+$).

TABLE II. Neutron resonances below 20 keV in ^{96}Zr(n,γ) as reported in Ref. [18]. Resonances analyzed in the present work are marked with an asterisk.

E_0 (keV)	J	l
0.301*	1/2	1
0.870		(1)
3.818*	1/2	1
4.133*	3/2	1
5.443*	1/2	0
5.971*	3/2	1
9.004*	(1/2)	1
13.278		1
15.138		1
15.419	1/2	0
17.779*	3/2	1

The second excited state, 1264 keV ($7/2^+$) is a 102 nanosecond isomer, so it is not likely to fall into the 10-ns coincidence window, and those events would fall outside of the cut on E_{total}. The state at 1400 keV has a tentative spin assignment of either $5/2^+$ or $3/2^+$ [20], but the fact that none of the $1/2^-$ capture states have any feeding to this state favors that this state is $5/2^+$. Since ^{96}Zr is stable, there are several ^{96}Zr(d, p) measurements, including measurements with a polarized deuteron beam [21]. The vector analyzing power measurements clearly indicate that the 1400 keV state should be $5/2^+$, which agrees with the present work. The simulations in the present work assume this spin. Above 1400 keV, the states are not well resolved by the resolution of DANCE, so reliable spectroscopic information cannot be extracted, and the information from Ref. [20] is assumed as is.

This work was motivated in part by a similar study [22] which measured the ^{238}U(n,γ) cross section using DANCE, and suggested some changes to the PSF of ^{239}U. In this case, with a very heavy nucleus with high level density, the two-step γ-ray cascades coming from several resonances all had very similar shapes. In the present work, as can be seen in Figure 2, the spectra, at least for $M_{\text{cl}} < 4$, significantly differ, even for resonances with the same J^π. This feature indicates that spectra from a single resonance will not likely result in a strong constraint on the PSF. Combining the information from several resonances with the same J^π should give a useful constraint, however, this requires a comparison with simulations that include these fluctuations.

V. γ-RAY CASCADE SIMULATIONS

The code DICEBOX [23] was used to simulate the γ-ray cascades from the capture state (neutron resonance), which

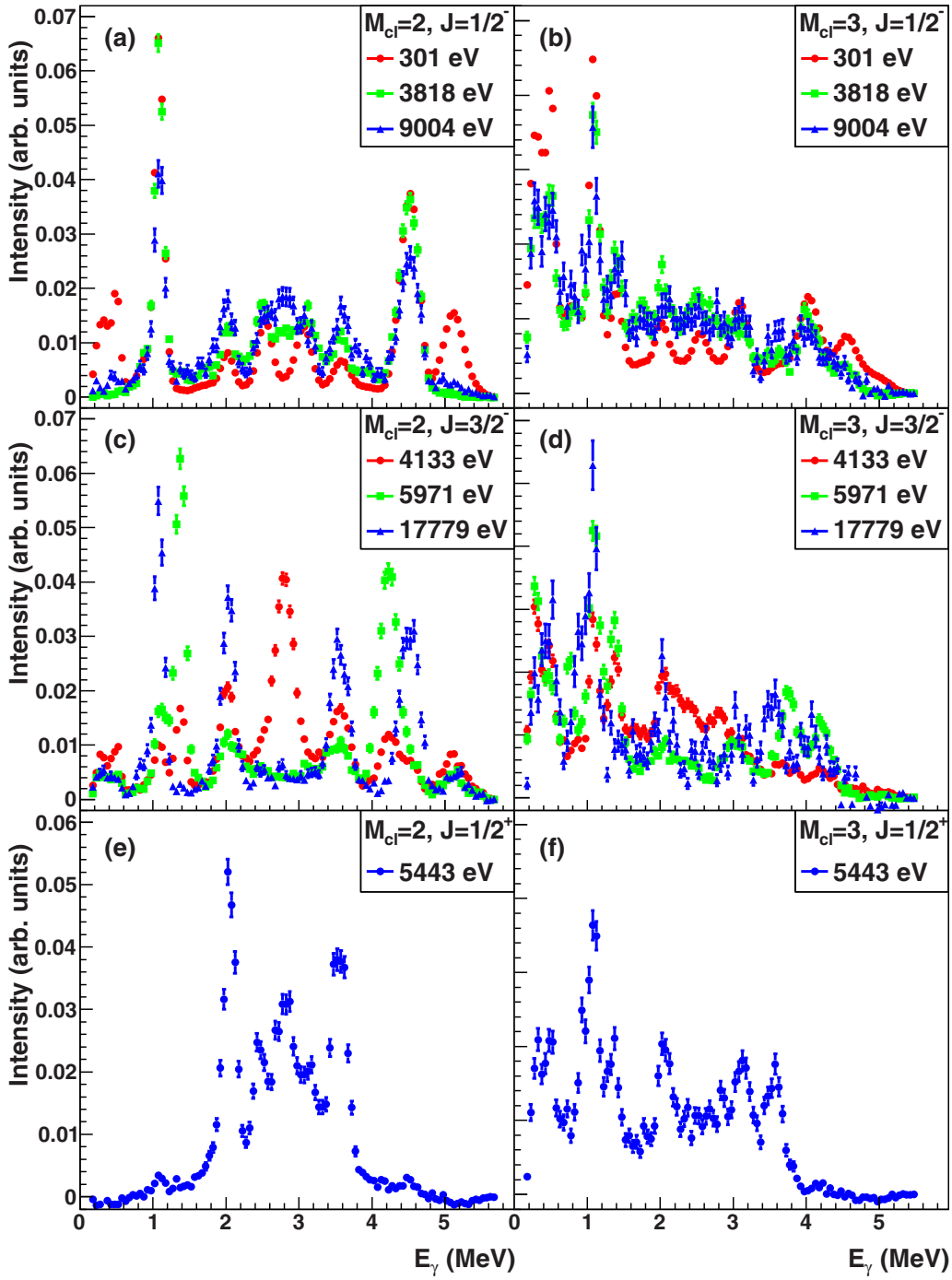

FIG. 2. Multistep-cascade spectra originating from ^{96}Zr(n,γ), for seven well-resolved resonances. The left panels (a), (c) and (e) show two-step cascades and the right panels (b), (d) and (f) show three-step cascades. The top (a), (b), middle (c), (d), and bottom (e), (f) panels group the resonances by the reported spin-parity of the capture states of $3/2^-$, $1/2^-$, and $1/2^+$, respectively.

is assumed to have a fixed energy, spin and parity. DICEBOX assumes that there is a critical energy, $E_{\rm crit}$, below which the energies, spins, parities, and branching ratios of all discrete levels are known. The properties of these known levels are taken from Ref. [20], but some changes are made based in the present experimental data, as discussed in the previous section. $E_{\rm crit} = 2.835$ MeV was used throughout this work. Above $E_{\rm crit}$, DICEBOX generates a random, discrete set of levels using a nuclear level density model. DICEBOX then uses a PSF model to generate a set of transition widths from each state to all other states below, as well as apply Porter-Thomas fluctuations to these widths. Because these discrete levels are generated randomly and so are not unique, a single set of levels and partial radiation widths is referred to as a nuclear realization, and average properties must be extracted from a large set of nuclear realizations. The number of realizations required to adequately characterize the distribution of γ-ray intensities depends on the

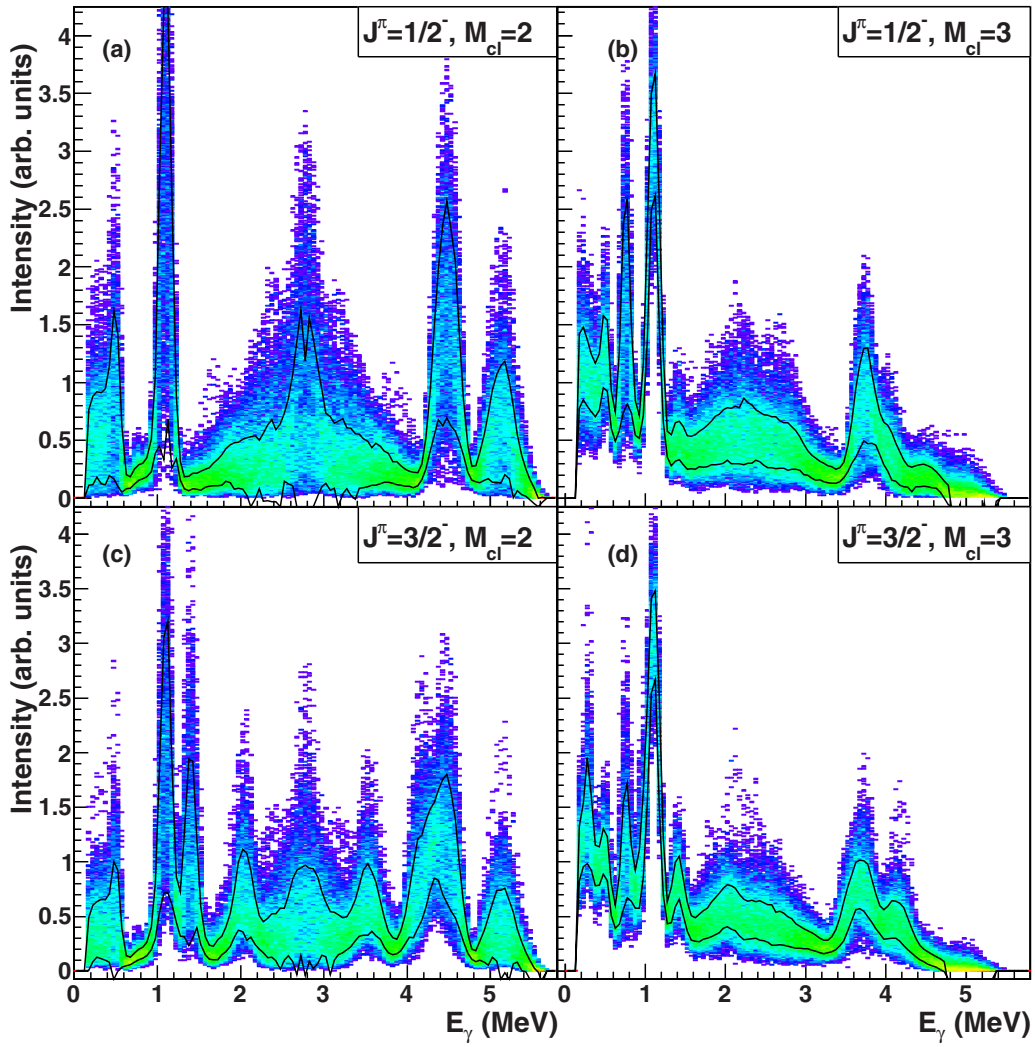

FIG. 3. Two-dimensional histogram showing the distribution of the γ-ray cascade spectra for 200 nuclear realizations, each with three subrealizations. Upper panels (a), (b) show DICEBOX results for $J^\pi = 1/2^-$ and lower panels (c), (d) show results for $J^\pi = 3/2^-$. The left panels (a), (c) show two step cascades and the right panels (b), (d) show three step cascades. The color scale shows the probability distribution of the intensities for each energy bin. The solid lines show the region that corresponds to the $x_0 \pm \sigma$, where x_0 and σ are the gaussian centroid and width parameters, obtained by fitting.

nucleus. For example, in Ref. [22], γ-ray cascades following ^{238}U(n,γ) were generated with 20 nuclear realizations, and data were compared to the spectrum consisting of the average γ-ray cascade of all 20 nuclear realizations. Because ^{97}Zr has much lower level density, the differences between realizations are more significant, so a larger number must be generated.

The experimental data for $J^\pi = 1/2^-$ and $3/2^-$ consist each of three resonances which have markedly different behavior. The decay of these resonances differs only in the intensities of γ-ray transitions, while the intensities of secondary transitions are the same. To take this behavior into account, the DICEBOX code was recently modified [24] with the introduction of *nuclear subrealizations*, which differ only by the intensities of primary transitions. Thus, each nuclear realization describes a possible version of the nucleus, and each subrealization represents a neutron resonance within that realization of the nucleus. In Ref. [24], a large (more than 10) number of resonances were measured for each of the two possible values of the capture state J^π, which allowed for a detailed check of the most probable transition intensities as well as their distribution about this central value. In the present work, having only three resonances for each spin does not allow for a precise check of these distributions. For the resonances with $J^\pi = 1/2^-$ and $J^\pi = 3/2^-$, we simulate three subrealizations for each nuclear realization and average them. With only one clearly identified resonance with $J^\pi = 1/2+$, no comparison between data and simulation for the $J^\pi = 1/2^+$ resonance will be presented. Finally, for a realistic comparison to the data, we can compare the average of the three measured resonances to the average behavior of 200 nuclear realizations, each made up of three sub-realizations. As described in Ref. [14], the γ-rays generated by DICEBOX are input to a GEANT4 simulation of the DANCE array which

TABLE III. Lorentzian parameters for the PSF used in the DICEBOX calculations.

	E_0 (MeV)	Γ_0 (MeV)	σ_0 (mb)
$E1$	16.39	4.92	209
$M1$	8.92	4.00	0.630
$E2$	13.71	4.95	1.98
LE $M1$	−1.0	3.0	1.0

reproduces the complete detector response, so that simulation and experiment can be compared directly.

Figure 3 shows the results of several DICEBOX calculations. For each subrealization, 100 000 γ-ray cascades were simulated. The number of realizations and the number of events are both sufficient to describe the γ-ray intensity distributions, while the number of sub-realizations is limited due to the experiment. The resulting cascade spectrum was normalized and added to a two-dimensional histogram. For each energy bin, a gaussian fit was done to extract the peak and width of the distribution, and this confidence band is shown by the solid lines in Fig. 3. The resulting distributions show that there is significant fluctuations in the simulated γ-ray cascades, which is consistent with the experimental spectra. The distribution of intensities of a specific γ-ray energy is somewhat asymmetric, because of the very small number of subrealizations being averaged, and so the plotted width is only an approximation here.

As mentioned above, differences in experimental spectra from different resonances are huge and may prevent strong constraints on the PSF. To test this expectation we made simulations with two very different PSF models. In the first (referred to as "Normal"), we used a simple standard Lorentzian shape for each multipolarity, which is given by Eq. (1) for $E1$ and $M1$, and Eq. (2) for $E2$. The parameters of the model are given in Table III, where E_0 is the centroid, Γ_0 is the width, and σ_0 is the maximum cross section of the Lorentzian lineshape, and the values are estimated from Ref. [25]. The second model mimics the low-energy enhancement of the PSF which is obtained from several "Oslo-type" experiments, where the PSF was determined using charged-particle induced reactions. To model this enhancement, we added an additional Lorentzian term to the $M1$ PSF with the parameters given in the last row of Table III. The magnitude of this enhancement is comparable to that observed in neighboring nuclei ($^{93-98}$Mo) in Ref. [7] with this PSF parametrization, which is shown in Fig. 4. The level density model used is the back-shifted Fermi gas model [26] with the parity-dependence of the level density taken from Ref. [27]. Although the level density model affects the calculated γ-ray cascades, it was held constant in this study as we are primarily comparing two drastically different PSF models:

$$f_{E1,M1}(E_\gamma) = \frac{1}{3(\pi\hbar c)^2}\frac{\sigma_0 E_\gamma \Gamma_0^2}{\left(E_\gamma^2 - E_0^2\right) + E_\gamma \Gamma_0^2}, \quad (1)$$

$$f_{E2}(E_\gamma) = \frac{1}{5(\pi\hbar c)^2}\frac{\sigma_0 \Gamma_0^2}{E_\gamma\left(\left(E_\gamma^2 - E_0^2\right) + E_\gamma \Gamma_0^2\right)}. \quad (2)$$

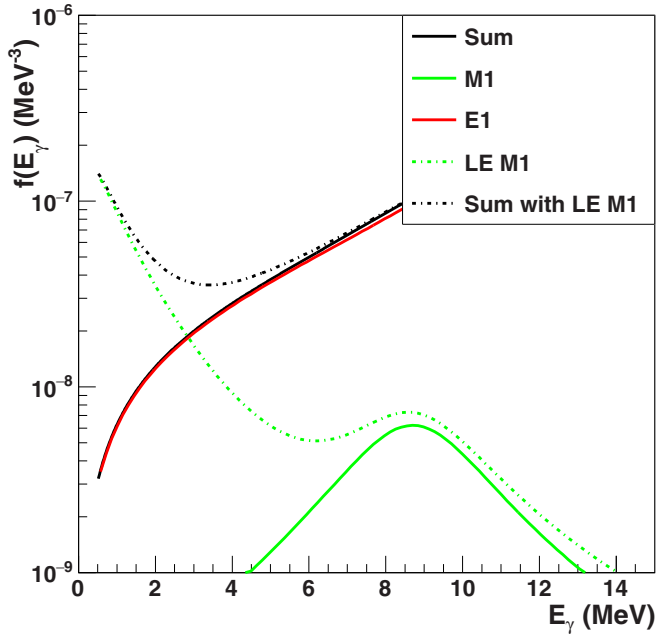

FIG. 4. Input PSF used for DICEBOX calculations in the present work. The solid red and green lines show the $E1$ and $M1$ components of the normal strength function, respectively, and the dashed green line shows the additional low energy $M1$ component that is under study here. The solid black line shows the sum of the normal $E1$ and $M1$ components, and the dashed black line shows the sum with the $M1$ low energy enhancement under investigation in this paper.

VI. COMPARISON OF RESULTS AND DISCUSSION

Figure 5 shows the comparison between the data and calculations with the two different PSF models shown in Fig. 4. The experimental and the simulated spectra are normalized to have the same area over the whole range of the figure. Because of the dramatic fluctuations in the DICEBOX results, especially for the two-step cascade spectra, the data are qualitatively consistent with both PSFs. This behavior confirms the expectation that it is difficult to obtain strong constraints on the PSF from the multistep-cascade spectra. Unfortunately, quantitative comparison between experiment and simulations is difficult, because the different multistep cascade spectra are not independent and each bin does not represent an independent variable. Also, the extracted width of the intensity distribution is only an approximation due to the distributions being asymmetric. Nonetheless, a simple χ^2 test can be done to attempt to extract the range of PSF with which the data agrees. To calculate the χ^2, for each bin, the squared difference between the mean intensity from DICEBOX and the experimental spectrum is divided by the width of the intensity distribution from DICEBOX and this quantity is summed over all bins, both J^π, and both multiplicities. The error in the experimental spectrum has a negligible contribution. This χ^2 test suggests that the σ_0 parameter for this $M1$ enhancement is less than 1.2 mb, at the one-sigma level. The result from this χ^2 test allows us to estimate the effect of this level of uncertainty in the PSF has on neutron capture cross sections, although this should only be seen as an approximate estimate.

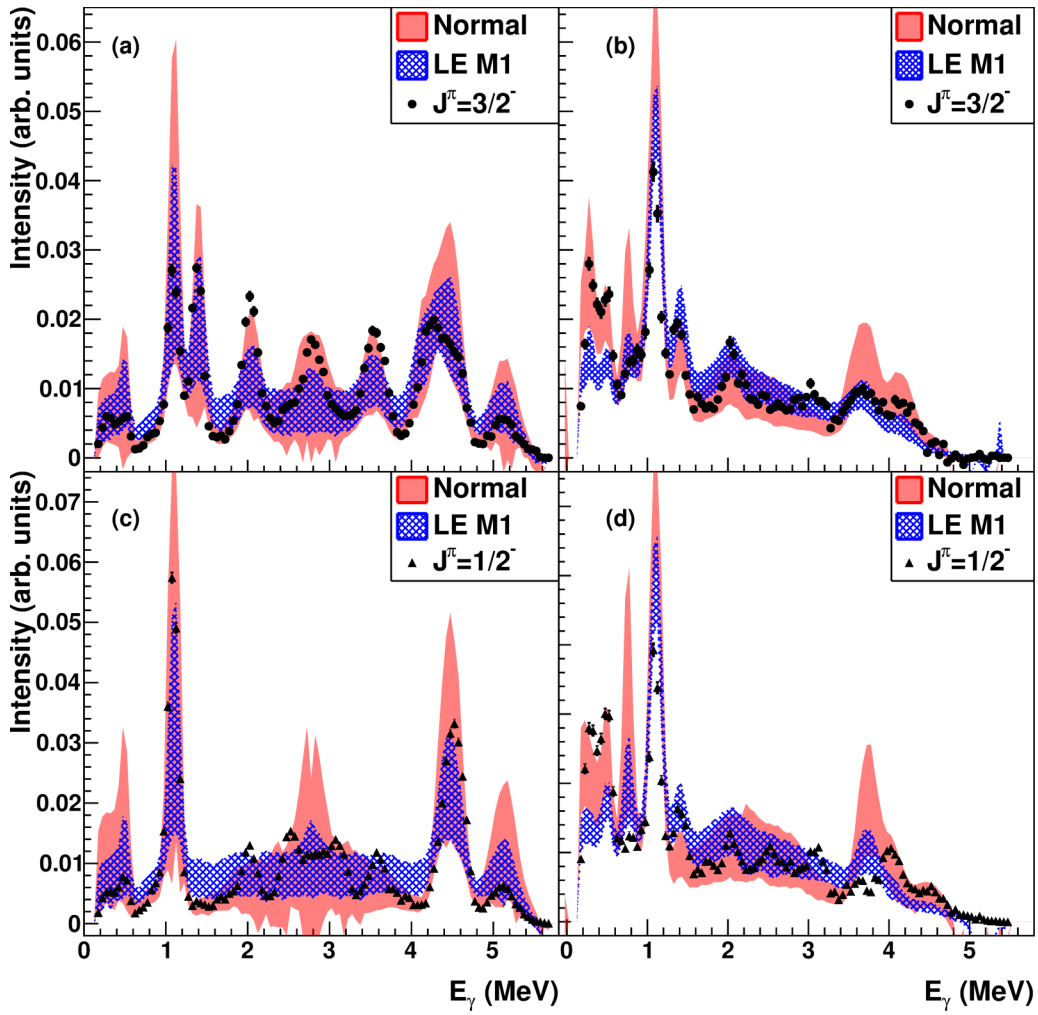

FIG. 5. DICEBOX simulation results compared to experimental data. Upper panels (a), (b) show the results for $J^\pi = 3/2^-$ and lower panels (c), (d) show the results for $J^\pi = 1/2^-$. The left panels (a), (c) show $M_{\rm cl} = 2$ and the right panels (b), (d) show $M_{\rm cl} = 3$. The data points consist of a mean of the three resonances measured for each spin. The solid red region shows the DICEBOX results using a normal PSF, while the hatched blue region shows the results calculated with a large low energy enhancement that has multipolarity $M1$. The experimental spectra and the simulated spectra are both normalized.

The spectra in Fig. 5 are all normalized to allow for a simple comparison of experiment to simulation, but the relative populations of $M_{\rm cl} = 2$ and $M_{\rm cl} = 3$ may also be sensitive to the PSF inputs, as in Ref. [24]. Figure 6 shows the relative multiplicity distributions for three resonances for each J^π compared to the results calculated with DICEBOX with the two different PSF models shown in Fig. 4. The multiplicity is calculated using the number of counts in the unnormalized multistep-cascade spectrum, so only includes the events which fall into the Q-value cut. All the multiplicity distributions are normalized so that $\sum(M_{\rm cl} = 2, 3, 4) = 1.0$. From this observable, there is an apparent preference for the "Normal" PSF model. The large fluctuations between resonances for $M_{\rm cl} = 1$ mean that this data point is not useful, but there is clear sensitivity for the $M_{\rm cl} = 2, 3, 4$, as the shapes of the distributions are different. The PSF model with the low-energy enhancement leads to more soft γ-ray transitions, which leads to a higher measured multiplicity. The experimental data are consistent with the normal PSF and suggest that a very large low-energy enhancement is not present in this nucleus.

The difficulty in this work is that the resonant neutron capture on ^{96}Zr populates a very limited number of resonances. Quantitative constraints on the PSF would be possible if the number of measured resonances was significantly higher, but resolving resonances with sufficient statistics above about 20 keV becomes intractable with current neutron time-of-flight facilities. In addition, the significant fluctuations between resonances indicates that trustworthy constraints will only be obtained using spectra only from the resonances that actually participate in the neutron capture reaction. The very loose constraint on the PSF that is shown in the present work will not be significantly improved with more careful measurements, rather, there is simply an acceptable range of PSF models that are equally consistent with the data. The wide range of acceptable PSF found in this experiment illustrates the limitations of using the statistical model to make predictions of neutron capture in cases of low nuclear level density or low

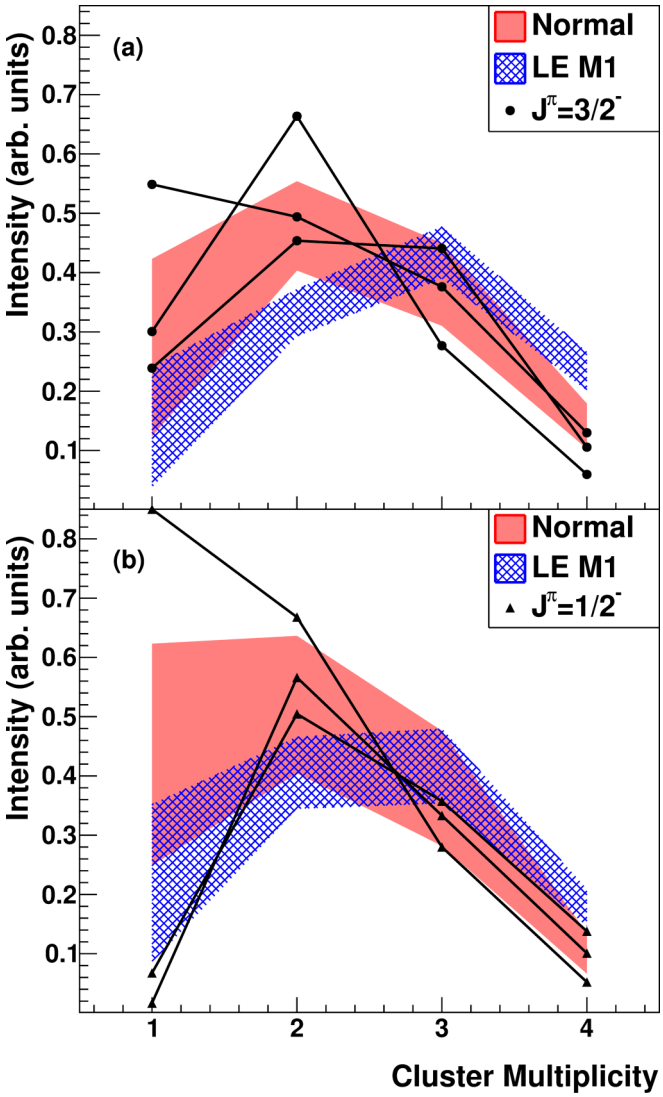

FIG. 6. (a) Multiplicity distributions for resonances with $J^\pi = 3/2^-$. The black symbols show the multiplicity distribution obtained from the data. The solid red region shows the DICEBOX results using a normal PSF, while the blue hatched region shows the results calculated with a large low energy enhancement that has multipolarity $M1$. (b) Multiplicity distributions for resonances with $J^\pi = 1/2^-$.

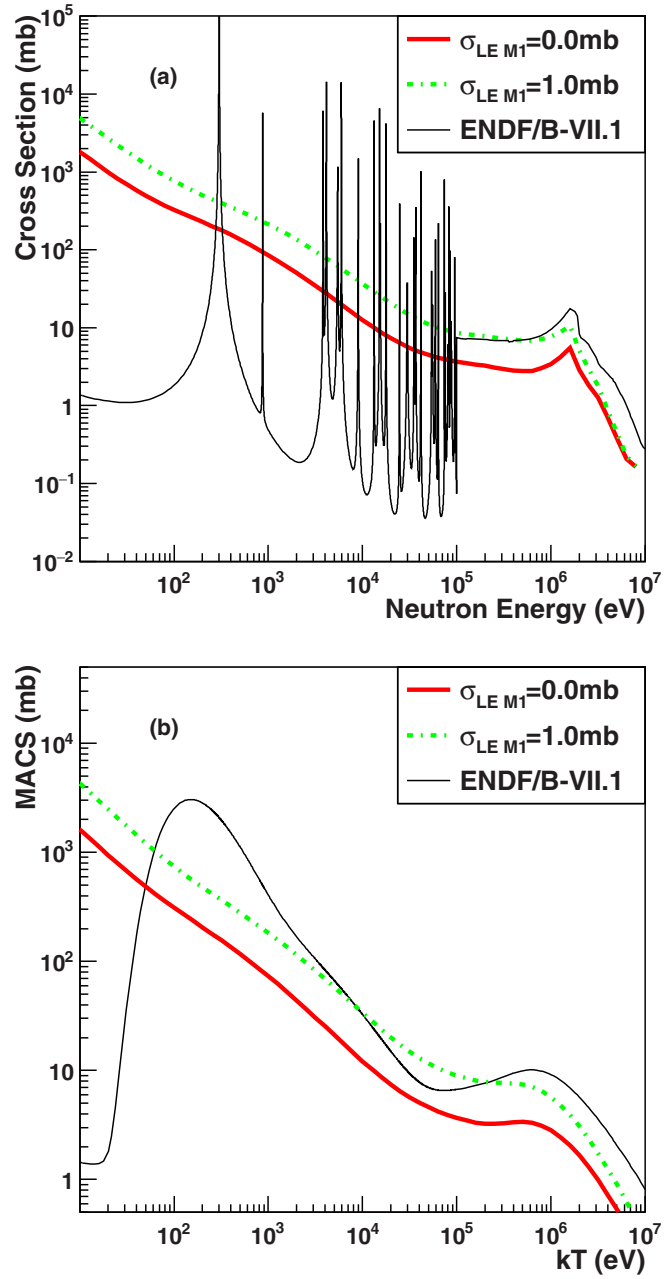

FIG. 7. (a) Radiative neutron capture cross section calculated using CoH_3 code. Solid red line corresponds to a PSF input with simple $E1$, $M1$, and $E2$ Lorentzian strength functions. Dashed green line corresponds to calculations with an $M1$ low energy enhancement, with a 1.0 mb strength as described in the text. The evaluated cross section from ENDF/B-VII.1 is shown in the solid black line. (b) Maxwellian averaged cross section (MACS) calculated using the CoH_3 results, as well the MACS calculated with the evaluated cross section.

neutron separation energy, because the large uncertainty in the PSF causes a large uncertainty in the predicted capture cross section.

To demonstrate the effect that these large uncertainties in the PSF have on the calculated neutron capture cross section, calculations using the CoH_3 [25] code were performed. The main features of the CoH_3 code relevant to this study are that it typically uses a generalized Lorentzian form for the strength function. To simplify the picture and to compare directly to the PSF models simulated using DICEBOX, the CoH_3 code was modified to use simple Lorentzian lineshapes for the present work. The result of the calculation is shown in Fig. 7. The top panel of Fig. 7 shows the CoH_3 calculation overlaid with the evaluated cross section, simply for reference. Comparing the CoH_3 results directly to the evaluated cross section in the resolved resonance region demonstrates that only a few resonances are actually contributing to the neutron capture cross section up to about 20 keV. Comparing the CoH_3 results for the two PSF models studied with DICEBOX, the uncertainty in the PSF extracted from the neutron capture cascades results in an uncertainty in the predicted capture cross section of a factor of 2–3. This uncertainty does not

come from a limitation of the experimental data, simply a consequence of applying the statistical model to a nucleus with low level density. The lower panel of Fig. 7 illustrates how the statistical model fails for very low level densities. Even when averaging over a large range of incident neutron energy, such as with the MACS, the result can be dominated by a few individual states, and so the cross section is poorly predicted using Hauser-Feshbach calculations.

VII. CONCLUSIONS AND OUTLOOK

Spectra of γ-ray cascades originating from the radiative neutron capture reaction ^{96}Zr(n,γ) were compared to simulated γ-ray cascades, in an attempt to constrain the low energy behavior of the PSF of ^{97}Zr, a nucleus with very low level density and low neutron separation energy. The resulting observables suggest that a low-energy enhancement may be present in the PSF but with a magnitude somewhat smaller than was investigated here. Information on this low-energy enhancement is especially important for nuclei with low neutron separation energy, as the enhancement of the neutron capture cross section can be significant. Due to large Porter-Thomas fluctuations in the transition strengths between the capture states and the low-lying states, the constraints on the PSF extracted from this type of measurement do not significantly constrain neutron capture predictions. When accounting for the large statistical fluctuations from one neutron resonance to another, the statistical model provides a reasonable description of the γ-ray cascade observables, but the physical process does not allow for precise capture predictions to be made using this model. Of course, this type of analysis is only sensitive to the shape of the PSF, and not the absolute value of the PSF, so the predictive power is limited still. For nuclei with low level density, different methods might be employed, such as indirect methods with charged particle induced reactions. Even if precise constraints on the *average* PSF can be measured using indirect methods, the large fluctuations between the individual capture states will be a significant source of error in the prediction of neutron capture cross sections. Moreover, because the reaction of interest is (n,γ), which populates a very limited range of J^{π} compared to charged particle induced reactions, the relevance of the PSF extracted from indirect methods must be investigated in further detail.

ACKNOWLEDGMENTS

This work benefited from the use of the LANSCE accelerator facility. Work was performed under the auspices of the U.S. Department of Energy by Los Alamos National Security, LLC under Contract No. DE-AC52-06NA25396.

[1] M. Mumpower, R. Surman, G. McLaughlin, and A. Aprahamian, Prog. Part. Nucl. Phys. **86**, 86 (2016).
[2] T. Rauscher and F.-K. Theilemann, Atom. Data Nucl. Data Tables **79**, 47 (2001).
[3] A. Koning, S. Hilaire, and M. Duijvestijn, Talys 1.8 (2006), www.talys.eu.
[4] D. Brink, Ph.D. thesis, Oxford University, 1955.
[5] J. Kopecky and R. Chrien, Nucl. Phys. A **468**, 285 (1987).
[6] A. Voinov, E. Algin, U. Agvaanluvsan, T. Belgya, R. Chankova, M. Guttormsen, G. E. Mitchell, J. Rekstad, A. Schiller, and S. Siem, Phys. Rev. Lett. **93**, 142504 (2004).
[7] M. Guttormsen, R. Chankova, U. Agvaanluvsan, E. Algin, L. A. Bernsteina, F. Ingebretsen, T. Lönnroth, S. Messelt, G. E. Mitchell, J. Rekstad *et al.*, Phys. Rev. C **71**, 044307 (2005).
[8] M. Wiedeking, L. A. Bernstein, M. Krtička, D. L. Bleuel, J. M. Allmond, M. S. Basunia, J. T. Burke, P. Fallon, R. B. Firestone, B. L. Goldblum *et al.*, Phys. Rev. Lett. **108**, 162503 (2012).
[9] M. Krtička, F. Bečvář, I. Tomandl, G. Rusev, U. Agvaanluvsan, and G. E. Mitchell, Phys. Rev. C **77**, 054319 (2008).
[10] S. A. Sheets, U. Agvaanluvsan, J. A. Becker, F. Bečvář, T. A. Bredeweg, R. C. Haight, M. Jandel, M. Krtička, G. E. Mitchell, J. M. O'Donnell *et al.*, Phys. Rev. C **79**, 024301 (2009).
[11] C. L. Walker, M. Krtička, B. Baramsai, F. Bečvář, T. A. Bredeweg, A. Chyzh, R. C. Haight, M. Jandel, J. Kroll, G. E. Mitchell *et al.*, Phys. Rev. C **92**, 014324 (2015).
[12] A. C. Larsen, M. Guttormsen, M. Krtička, E. Běták, A. Bürger, A. Görgen, H. T. Nyhus, J. Rekstad, A. Schiller, S. Siem *et al.*, Phys. Rev. C **83**, 034315 (2011).
[13] A. C. Larsen and S. Goriely, Phys. Rev. C **82**, 014318 (2010).
[14] M. Jandel, T. Bredeweg, A. Couture, M. Fowler, E. Bond, M. Chadwick, R. Clement, E.-I. Esch, J. O'Donnell, R. Reifarth *et al.*, Nucl. Instr. Meth. B **261**, 1117 (2007).
[15] P. Lisowski, C. Bowman, G. Russell, and S. Wender, Nucl. Sci. Eng. **106**, 208 (1990).
[16] M. Jandel, T. A. Bredeweg, E. M. Bond, M. B. Chadwick, R. R. Clement, A. Couture, J. M. O'Donnell, R. C. Haight, T. Kawano, R. Reifarth *et al.*, Phys. Rev. C **78**, 034609 (2008).
[17] S. Mosby, T. A. Bredeweg, A. Chyzh, A. Couture, R. Henderson, M. Jandel, E. Kwan, J. M. O'Donnell, J. Ullmann, and C. Y. Wu, Phys. Rev. C **89**, 034610 (2014).
[18] S. Mughabghab, *Atlas of Neutron Resonances* (Elsevier, Amsterdam, 2006).
[19] G. Tagliente, P. M. Milazzo, K. Fujii, U. Abbondanno, G. Aerts, H. Álvarez, F. Alvarez-Velarde, S. Andriamonje, J. Andrzejewski, L. Audouin *et al.*, Phys. Rev. C **84**, 055802 (2011).
[20] N. Nica, Nuclear Data Sheets **111**, 525 (2010).
[21] D. Hennies, Ph.D. thesis, University of Wisconsin-Madison, 1980.
[22] J. L. Ullmann, T. Kawano, T. A. Bredeweg, A. Couture, R. C. Haight, M. Jandel, J. M. O'Donnell, R. S. Rundberg, D. J. Vieira, J. B. Wilhelmy *et al.*, Phys. Rev. C **89**, 034603 (2014).
[23] F. Bečvář, Nucl. Instrum. Methods Phys. Res. Sec. A: Accel., Spectr., Detect. Assoc. Equip. **417**, 434 (1998).
[24] S. Valenta, B. Baramsai, T. A. Bredeweg, A. Couture, A. Chyzh, M. Jandel, J. Kroll, M. Krtička, G. E. Mitchell, J. M. O'Donnell *et al.*, Phys. Rev. C **96**, 054315 (2017).
[25] T. Kawano, P. Talou, M. B. Chadwick, and T. Watanabe, J. Nucl. Sci. Technol. **47**, 462 (2010).
[26] T. von Egidy and D. Bucurescu, Phys. Rev. C **72**, 044311 (2005).
[27] S. I. Al-Quraishi, S. M. Grimes, T. N. Massey, and D. A. Resler, Phys. Rev. C **67**, 015803 (2003).